TECHNICAL REPORT ARBRL-TR-02465

TWO-PHASE VISCOUS FLOW MODELING OF INTERIOR BALLISTICS, ALGORITHM, AND NUMERICAL PREDICTIONS FOR AN IDEALIZED LAGRANGE GUN

James A. Schmitt
Norman E. Banks
Csaba K. Zoltani
Thomas L. Mann
Howard J. Gibeling

January 1983

US ARMY ARMAMENT RESEARCH AND DEVELOPMENT COMMAND
BALLISTIC RESEARCH LABORATORY
ABERDEEN PROVING GROUND, MARYLAND

Destroy this report when it is no longer needed.
Do not return it to the originator.

Secondary distribution of this report is prohibited.

Additional copies of this report may be obtained from the National Technical Information Service, U. S. Department of Commerce, Springfield, Virginia 22161.

The findings in this report are not to be construed as an official Department of the Army position, unless so designated by other authorized documents.

The use of trade names or manufacturers' names in this report does not constitute indorsement of any commercial product.

UNCLASSIFIED

SECURITY CLASSIFICATION OF THIS PAGE (When Data Entered)

REPORT DOCUMENTATION PAGE	READ INSTRUCTIONS BEFORE COMPLETING FORM
1. REPORT NUMBER: Technical Report ARBRL-TR-02465	2. GOVT ACCESSION NO.: AD-A125 336
3. RECIPIENT'S CATALOG NUMBER	
4. TITLE (and Subtitle): Two-Phase Viscous Flow Modeling of Interior Ballistics, Algorithm, and Numerical Predictions for an Idealized Lagrange Gun	5. TYPE OF REPORT & PERIOD COVERED: Technical Report
	6. PERFORMING ORG. REPORT NUMBER
7. AUTHOR(s): James A. Schmitt, Norman E. Banks, Csaba K. Zoltani, Howard J. Gibeling*, Thomas L. Mann	8. CONTRACT OR GRANT NUMBER(s)
9. PERFORMING ORGANIZATION NAME AND ADDRESS: US Army Ballistic Research Laboratory, ATTN: DRDAR-BLI, Aberdeen Proving Ground, MD 21005	10. PROGRAM ELEMENT, PROJECT, TASK AREA & WORK UNIT NUMBERS: 1L161102AH43
11. CONTROLLING OFFICE NAME AND ADDRESS: US Army Armament Research and Development Command, US Army Ballistic Research Laboratory (DRDAR-BL), Aberdeen Proving Ground, MD 21005	12. REPORT DATE: January 1983
	13. NUMBER OF PAGES: 38
14. MONITORING AGENCY NAME & ADDRESS (if different from Controlling Office)	15. SECURITY CLASS. (of this report): UNCLASSIFIED
	15a. DECLASSIFICATION/DOWNGRADING SCHEDULE

16. DISTRIBUTION STATEMENT (of this Report)

Approved for public release; distribution unlimited.

17. DISTRIBUTION STATEMENT (of the abstract entered in Block 20, if different from Report)

18. SUPPLEMENTARY NOTES

*Scientific Research Associates, Inc.
Glastonbury, CT 06033

19. KEY WORDS (Continue on reverse side if necessary and identify by block number)

Interior Ballistics	ALPHA	Adiabatic Wall
Lagrange Gun	Laminar	
Two-Phase	Turbulence	
Viscous Flow	Isothermal Wall	

20. ABSTRACT (Continue on reverse side if necessary and identify by block number) dll

A new state of the art algorithm, ALPHA, for the simulation of the multiphase, multidimensional, unsteady, compressible, viscous, non-reactive, interior ballistics flow in a gun tube behind an accelerating projectile is described. The paper contains discussions of the physical processes in a real gun environment, of the mathematical model of these phenomena, and of the numerical technique for solving the equations. The algorithm allows the inclusion of several submodels, such as, heat transfer and (CONTINUED)

DD FORM 1 JAN 73 1473 EDITION OF 1 NOV 65 IS OBSOLETE

UNCLASSIFIED

SECURITY CLASSIFICATION OF THIS PAGE (When Data Entered)

20. ABSTRACT (Continued):

turbulence. This permits the determination of the effects of these submodels on the flow. Numerical results of an idealized, one-phase ballistic cycle are given. Some of the significant results include the existence of a concentrated region of high temperature near the juncture of the projectile base and tube wall, the increase of the displacement thickness by a factor of at least three over most of the tube's length when turbulence effects are included, and the degradation of the projectile velocity by approximately ten percent under an isothermal cold wall condition.

TABLE OF CONTENTS

LIST OF FIGURES

I. INTRODUCTION

To advance the state-of-the-art of gun system development, especially those with high muzzle velocity, a detailed understanding of the phenomena occurring within the gun tube is needed. Current theoretical and experimental research at the Interior Ballistics Division of the Ballistic Research Laboratory and Scientific Research Associates, Inc., addresses this problem with special emphasis on the modeling of the unsteady, multiphase aspect of the interior ballistic flows. The ballistic cycle, as illustrated in Figure 1,[1] commences with the ignition of the propellant charge and terminates with the exit of the projectile and the emptying of the hot gases and any unburned propellant from the gun tube. Typically, an ignition of the propellant bed is started by a hot, gas-particle flow from the igniter. As the flame spreads throughout the propellant bed, gases are generated, pressure waves evolve, fluidization of the propellant bed begins, and subsequently, this multiphase flow proceeds down the tube behind the nonuniformly accelerated projectile. Once there is appreciable axial projectile displacement, several ancillary phenomena can be observed. These include projectile/tube interaction manifested by balloting and tube vibration as well as the leakage of propellant gases around and ahead of the moving projectile. These processes are not considered in this report.

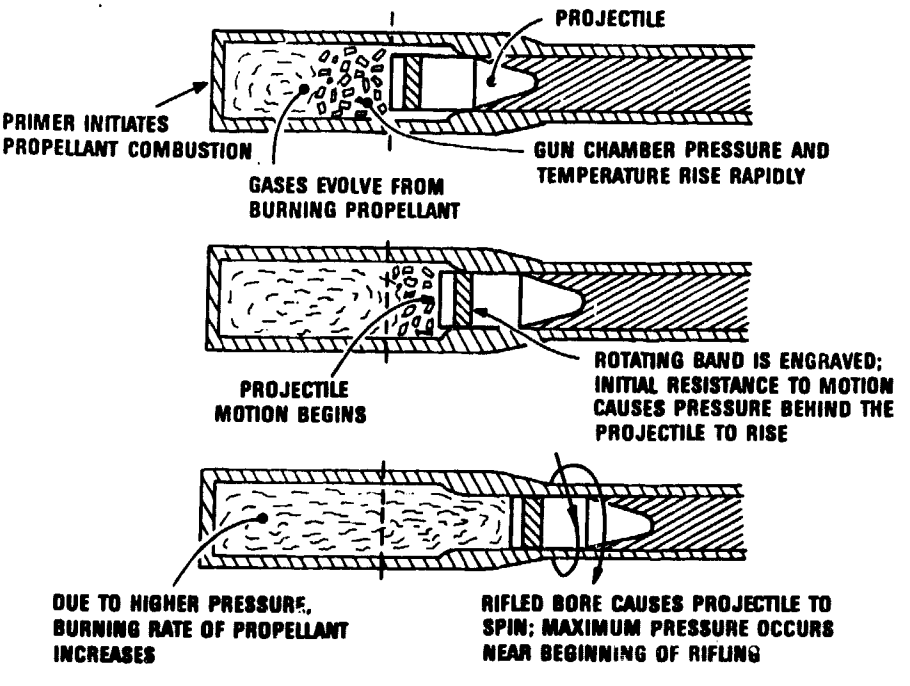

Figure 1. Illustration of the Ballistic Cycle (Adaptation from Ref. 1)

[1] *H. Krier and M. Adams, "An Introduction to Gun Interior Ballistics and a Simplified Ballistic Code," Interior Ballistics of Guns, H. Krier and M. Summerfield, Eds., Progress in Astronautics and Aeronautics, Vol. 66, pp. 1-36, 1979.*

Our interest is focused on the flow within a gun bounded by the breech, the gun tube wall, and the projectile base. From a global point of view, interior ballistics phenomena can be divided into two coupled parts: the two-phase flow behind the projectile and the motion of the projectile. The two-phase flow provides a force which partially determines the motion of the projectile, and the projectile base is an accelerating boundary for the two-phase flow field. From our standpoint, the projectile motion can be treated by a lumped parameter analysis in which the projectile moves axially with a possible fixed rotation, if in a rifled gun tube, and with a perfect seal and no gas leakage. Applying Newton's second law to the projectile axial motion, we obtain an ordinary differential equation. The forces on the projectile include the area integral of the pressure at the base of the projectile plus the wall friction force, the force needed to engrave the rotating bands on the grooves of a rifled gun tube, the rotational force, and the air resistance. The last four forces are usually prescribed for a given gun and projectile.

Until recently, the most sophisticated modeling of major portions of the ballistic cycle has been limited to quasi-one-dimensional, inviscid, two-phase flow analyses[2-5]. By assuming a cylindrically symmetric flow, parts of the ballistic cycle can now be modeled two-dimensionally. Gough[6] has recently developed an inviscid, two-dimensional model to study these phenomena. ALPHA[7,8] is the first two-phase, two-dimensional, Navier-Stokes model developed to simulate the ballistic cycle. None of the above models includes chemical effects.

---

[2] *P.S. Gough and F.J. Zwarts, "Modeling Heterogeneous Two-Phase Reacting Flow," AIAA Journal, Vol. 17, No. 1, pp. 17-25, 1979.*

[3] *K.K. Kuo, J.H. Koo, T.R. Davis, and G.R. Coates, "Transient Combustion in Mobile Gas-Permeable Propellants," Acta Astronautica, Vol. 3, pp. 573-591, 1976.*

[4] *E.B. Fisher, K.W. Graves, and A.P. Trippe, "Application of a Flame Spread Model to Design Problems in the 155-mm Propelling Charge," 12th JANNAF Combustion Meeting, CPIA Pub. 273, Vol. I, pp. 199-219, December 1975.*

[5] *H. Krier and S.S. Gokhale, "Modeling of Convective Mode Combustion Through Granulated Propellant to Predict Detonation Transition," AIAA Journal, Vol. 16, No. 2, pp. 177-183, 1978.*

[6] *P.S. Gough, "A Two-Dimensional Model of the Interior Ballistics of Bagged Artillery Charges," USA ARRADCOM/Ballistic Research Laboratory, Aberdeen Proving Ground, MD, ARBRL-CR-00452, April 1981.*

[7] *H.J. Gibeling, R.C. Buggeln, and H. McDonald, "Development of a Two-Dimensional Implicit Interior Ballistics Code," USA ARRADCOM/Ballistic Research Laboratory, Aberdeen Proving Ground, MD, ARBRL-CR-00411, January 1980.*

[8] *H.J. Gibeling and H. McDonald, "Development of a Two-Dimensinal Implicit Interior Ballistics Code," USA ARRADCOM/Ballistic Research Laboratory, Aberdeen Proving Ground, MD, ARBRL-CR-00451, March 1981.*

The purpose of this report is to present a two-phase, viscous model and to detail the calculations for an idealized one-phase ballistic cycle. Although these first applications of ALPHA exclude the second phase, important effects of the basic mechanisms of heat transfer to the gun tube wall and of a turbulent flow are isolated and resolved. In Section II, the governing equations which provide a model of the two-phase interior ballistics flow are listed. The description of the numerical scheme to solve these equations is also given. The results of three simulations: the laminar flow-adiabatic wall, the turbulent flow-adiabatic wall, and the laminar flow-isothermal wall, are then presented. Section V assays the results and discusses future work.

II. GOVERNING EQUATIONS

Because of the complex nature of the two-phase flow behind the projectile, simplifying assumptions must be made prudently in order that significant phenomena are not neglected in the model. Therefore, we start with a general formulation and introduce simplifications only when warranted. Due to the large number of propellant grains, of the order of a few thousands, the mathematical description is restricted to the bulk or average properties of the flow. An averaged variable represents the integral of the product of a microscopic variable and a weighting function, which reflects the influence of remote points on the average value, over time and space. Likewise, the equations of continuum mechanics are replaced with a set of averaged equations in the averaged variables at each spatial position and time. The derivation of these averaged equations is discussed in Refs. 7 and 8. The constitutive laws represent relations between the averaged variables and the different phases, and are given in the Appendix. The averaged, Navier-Stokes equations are summarized here in dimensional form.

The gas and solid phase continuity equations are

$$\frac{\partial(\alpha\rho)}{\partial t} + \nabla \cdot (\alpha\rho\vec{U}) = \Gamma \quad , \tag{1}$$

and

$$\frac{\partial(1-\alpha)}{\partial t} + \nabla \cdot [(1-\alpha)\,\vec{U}_p] = -\frac{\Gamma}{\rho_p} \quad , \tag{2}$$

respectively, where the porosity α is the ratio of volume occupied by the gas phase to the total volume. The averaged densities and velocities of the gas and solid phases are denoted by ρ, $\vec{U}$, ρ_p, $\vec{U}_p$, respectively. The interphase mass transfer for the gas, Γ, is due to the burning propellant and is given by Eq. (19). (Eqs. (19) through (40) are in the Appendix.) The gas and solid phase momentum equations are

$$\frac{\partial(\alpha\rho\vec{U})}{\partial t} + \nabla \cdot (\alpha\rho\vec{U}\vec{U}) = - \alpha\nabla P + \nabla \cdot [\alpha(\bar{\bar{\pi}} + \bar{\bar{\pi}}^T)] - (1-\alpha) \frac{S_p}{V_p} \langle\vec{F}\rangle + \vec{U}_p \Gamma \quad , \tag{3}$$

and

$$\frac{\partial[(1-\alpha)\rho_p \vec{U}_p]}{\partial t} + \nabla \cdot [(1-\alpha)\rho_p \vec{U}_p \vec{U}_p] = - (1-\alpha)\nabla P + \nabla [(1-\alpha)R_p] + (1-\alpha) \frac{S_p}{V_p} \langle\vec{F}\rangle - \vec{U}_p \Gamma \quad , \tag{4}$$

where P is the averaged pressure. The tensors, $\bar{\bar{\pi}}$ and $\bar{\bar{\pi}}^T$, Eqs. (23) and (26), are the laminar and turbulent stress tensors, respectively. The constitutive relations for grain surface area, S_p, and volume, V_p, the interphase drag relation, $\langle\vec{F}\rangle$, and the intergranular stress relation, R_p, are given by Eqs. (20), (21), (29), and (30), respectively. The velocity vectors, $\vec{U}$ and $\vec{U}_p$, have three components; a radial, an axisymmetric angular, and an axial. Axisymmetric swirl may be important for the case of the projectile rotation. The gas phase energy equation is

$$\frac{\partial(\alpha\rho h)}{\partial t} + \nabla \cdot (\alpha\rho\vec{U}h) = - \nabla \cdot [\alpha(\vec{q} + \vec{q}^T)] + \frac{D}{Dt}(\alpha P) + \alpha\Phi + \alpha\rho\varepsilon + \Lambda \quad , \tag{5}$$

where h is the enthalpy of the gas. The dissipation function, Φ, the turbulent kinetic energy dissipation rate, ε, the energy transfer term between the solid and gas phases, Λ, and the laminar and turbulent heat flux vectors $\vec{q}$ and $\vec{q}^T$ are given by Eqs. (31), (28), (32), (34), and (35), respectively. The symbol D/Dt denotes the material derivative. The Noble-Abel equation of state, (38), is used for the gas. The turbulent kinetic energy is given by

$$\frac{\partial(\alpha\rho k)}{\partial t} + \nabla \cdot (\alpha\rho\vec{U}k) = \nabla \cdot (\alpha \frac{\mu^T}{\sigma_k} \nabla k) + \alpha \{\mu^T [2\bar{\bar{D}}:\bar{\bar{D}} - \frac{2}{3}(\nabla\cdot\vec{U})^2] - \frac{2}{3}\rho k \nabla\cdot\vec{U} - \rho\varepsilon\} \quad , \tag{6}$$

where σ_k is set equal to one. The rate of strain tensor $\bar{\bar{D}}$ and the turbulent viscosity μ^T are given by Eqs. (24) and (27), respectively.

By excluding the chemical reactions in the present two-phase flow analysis, the gas phase species and gasified propellant species mass fractions are not required. However, in order to consider the effects of several types of propellants within the tube, transport equations for the reciprocal of the

gas mixture molecular weight M and specific heat at constant pressure c_p are solved. The governing equations for M and c_p are

$$\frac{\partial(\alpha\rho M)}{\partial t} + \nabla \cdot (\alpha\rho\vec{U}M) = \nabla \cdot [\alpha\Gamma_m \nabla M] + M_p\dot{\Gamma} \quad , \tag{7}$$

and

$$\frac{\partial(\alpha\rho c_p)}{\partial t} + \nabla \cdot (\alpha\rho\vec{U}c_p) = \nabla \cdot [\alpha\Gamma_m \nabla c_p] + (c_p)_p\dot{\Gamma} \quad , \tag{8}$$

where M_p and $(c_p)_p$ are the reciprocal molecular weight and specific heat at constant pressure of the propellant, respectively, $\Gamma_m = \mu_{eff}/Sc_{eff}$, $\mu_{eff} = \mu + \mu^T$, and $Sc_{eff} = 0.9$.

Presently, we assume that the propellant grains are spherical. To determine ignition, the surface temperature of these spheres must be calculated. If we assume that the penetration depth of the thermal wave into the grain is small compared to the grain diameter, a one-dimensional approximation can be used to obtain the propellant surface temperature. The appropriate equation for the propellant temperature T_p is

$$\left(\frac{DT_p}{Dt}\right)_{\tilde{r}} = \frac{d_p}{\tilde{r}^2} \frac{\partial^2(\tilde{r}^2 T_p)}{\partial \tilde{r}^2} \quad , \tag{9}$$

where $\tilde{r}$ is the radial location within the spherical grain and d_p is its thermal diffusivity. Once the surface temperature of the grain exceeds the ignition temperature of the propellant, the propellant grain is assumed to burn until it is completely consumed. The actual burning is modeled as a regression of the surface of the propellant which results in the deposition of mass, momentum, and energy into the gas. The equation for the particle radius, r_p, including turbulent diffusion, is

$$\frac{\partial r_p}{\partial t} + \vec{U}_p \cdot \nabla r_p = \frac{1}{(1-\alpha)\rho_p} \nabla \cdot [(1-\alpha)\Gamma_m \nabla r_p] - \langle d \rangle \quad , \tag{10}$$

where the regression rate $\langle d \rangle$ is given by Eq. (22).

The effects of the primer which deposits hot gases into the propellant bed to begin ignition can be modeled in several ways. One approach is to treat the "primer source" as a boundary condition or initial condition either near the tube centerline for a center core igniter or near the breech end for a base igniter[9].

---

[9] *D. Drew, Rensselaer Polytechnic Institute, Private Communication, June 1981.*

The two-phase governing equations, Eqs. (1) through (8) and (10), are written as a general system of time-dependent nonlinear partial differential equations. The dependent variables are: the components of gas and solid phase velocities $\vec{U}$, $\vec{U}_p$, partial densities $\alpha\rho$, $(1-\alpha)\rho_p$, gas phase static enthalpy, h, specific heat, c_p, reciprocal mixture molecular weight, M, the turbulent kinetic energy, k, and solid phase particle radius, r_p. Subsequent to the solution of this coupled system of gas-solid phase equations, the solid particle surface temperature is determined from the solution of Eq. (9).

III. ALGORITHM DESCRIPTION

For the algorithm an implicit formulation is favored in view of the desired boundary layer resolution along the gun barrel. To treat the nonlinearities of the governing equations, Taylor-series expansions in time are used to linearize the system to the same order accuracy as the temporal discretization. To efficiently eliminate the large block banded matrix, a splitting of the matrix into a sequence of more easily treated component matrices is performed. Because of this construction, the resulting algorithm is termed a split linearized block implicit (LBI) scheme.

The numerical algorithm is described in detail in Refs. 10 and 11. Following Ref. 12, a brief derivation of the scheme, which includes consideration of intermediate boundary conditions required by split schemes, is now given. By considering these intermediate boundary conditions, a commutative condition on the boundary conditions is identified and it is shown that the treatment of these intermediate boundary conditions can affect transient accuracy, and may even cause errors in steady solutions.

To illustrate the derivation, let

$$(\vec{\phi}^{n+1} - \vec{\phi}^{n})/\Delta t = \beta D(\vec{\phi}^{n+1}) + (1-\beta)D(\vec{\phi}^{n}) + O[\Delta t^2, (\beta-1/2)\Delta t] \qquad (11)$$

approximate $\partial\vec{\phi}/\partial t = D(\vec{\phi})$, a system of time-dependent nonlinear partial differential equations for the vector $\vec{\phi}$ of dependent variables, where D is a multidimensional vector spatial differential operator, and t is a time

---

[10] *W.R. Briley and H. McDonald, "Solution of the Multidimensional Compressible Navier-Stokes Equations by a Generalized Implicit Method," Journal of Computational Physics, Vol. 24, No. 4, pp. 372-397, 1977.*

[11] *W.R. Briley and H. McDonald, "On the Structure and Use of Linearized Block ADI and Related Schemes," Journal of Computational Physics, Vol. 34, No. 1, pp. 54-73, 1980.*

[12] *H. McDonald and W.R. Briley, "Some Observations on Numerical Solutions of the Three-Dimensional Navier-Stokes Equations," presented at Symposium on Numerical and Physical Aspects of Aerodynamic Flows, California State University, Long Beach, CA, 1981.*

variable with discretization $\Delta t = t^{n+1} - t^n$. A local time linearization of requisite formal accuracy is introduced. This serves to define a linear differential operator L such that

$$D(\vec{\phi}^{n+1}) = D(\vec{\phi}^n) + L^n (\vec{\phi}^{n+1} - \vec{\phi}^n) + O(\Delta t^2) \quad . \tag{12}$$

Thus, Eq. (11) can be written as the linear system

$$(I - \beta \Delta t L^n) (\underset{\sim}{\vec{\phi}}^{n+1} - \vec{\phi}^n) = \Delta t D(\vec{\phi}^n) \quad , \tag{13a}$$

$$\underset{\sim}{\vec{\phi}}^{n+1} - \vec{\phi}^n = \vec{\phi}^{n+1} - \vec{\phi}^n + O[\Delta t^3, (\beta - 1/2)\Delta t^2] \quad , \tag{13b}$$

where $\underset{\sim}{\vec{\phi}}^{n+1}$ differs from $\vec{\phi}^{n+1}$ by the linearization error.

To obtain a split scheme, the multidimensional operation L is divided into m "one-dimensional" suboperators $L = L_1 + L_2 + \ldots + L_m$ which are usually associated with coordinate directions. For simplicity, only two suboperators are considered here: inclusion of additional suboperators is straightforward. Eq. (13) can then be replaced by the approximate factorization

$$(I - \beta \Delta t L_1^n) \quad (I - \beta \Delta t L_2^n) \quad (\vec{\phi}^* - \vec{\phi}^n) = \Delta t \; D(\vec{\phi}^n) \quad , \tag{14a}$$

$$\vec{\phi}^* - \vec{\phi}^n = \underset{\sim}{\vec{\phi}}^{n+1} - \vec{\phi}^n + O[\Delta t^3, (\beta - 1/2)\Delta t^2] \quad , \tag{14b}$$

where $\vec{\phi}^*$ differs from $\underset{\sim}{\vec{\phi}}^{n+1}$ by the factorization error. Although $\vec{\phi}^*$, $\underset{\sim}{\vec{\phi}}^{n+1}$, and $\vec{\phi}^{n+1}$ are interchangeable without formal loss of accuracy, the distinction is worthwhile, since they entail different types of error which in practice may differ widely in magnitude. Note that the approximate factorization (14a) does not represent a simplification of Eq. (13) until it is written in a split form.

The most obvious splitting of Eq. (14a) is

$$(I - \beta \Delta t L_1^n) \; \vec{\psi} = \Delta t \; D(\vec{\phi}^n) \quad , \tag{15a}$$

$$(I - \beta \Delta t L_2^n) \quad (\vec{\phi}^* - \vec{\phi}^n) = \vec{\psi} \quad , \tag{15b}$$

where $\vec{\psi}$ is an intermediate quantity whose physical significance follows from its definition (15b), which implies that $\vec{\psi}$ approximates the time increment $\vec{\phi}^{n+1} - \vec{\phi}^n$ to order Δt. If spatial derivatives appearing in L_1 and L_2 are replaced by three-point difference formulas, then each step in Eqs. (15a) and (15b) can be solved by a block-tridiagonal elimination.

The derivation of the algorithm is incomplete, however, since Eq. (15a) cannot be solved for $\vec{\psi}$ without deriving boundary conditions for $\vec{\psi}$ from those given for $\vec{\phi}$. If function values of $\vec{\phi}$ are given, then boundary values of $\vec{\psi}$ can always be derived from the definition (15b) of $\vec{\psi}$ for use in Eq. (15a). In practice, however, more complex boundary conditions, such as normal derivatives, may be specified; and so, here we consider a much more general nonlinear boundary condition which, after linearization as in Eq. (12), can be written in the form $B^n(\vec{\phi}^{n+1}) = \vec{g}(t,\vec{\phi}^n)$. Here, B^n is a linearized operator which may include the same derivatives as L_2^n, and g is given. Applying the operator B to Eq. (15b) gives

$$B^n(\vec{\psi}) = B^n(\vec{\phi}^* - \vec{\phi}^n) - \beta\Delta t\, B^n[L_2^n(\vec{\phi}^* - \vec{\phi}^n)] \quad . \tag{16}$$

Since $B^n(\vec{\phi}^* - \vec{\phi}^n) \tilde{=} g^{n+1} - g^n$ without formal loss of accuracy, Eq. (16) can be used to derive exact boundary conditions for $\vec{\psi}$ from the given boundary conditions <u>provided</u> B^n and L_2^n commute, which is unfortunately often not the case. The need for commutativity occurs because $L_2^n\,\vec{\phi}^*$ cannot be computed at this step in the algorithm, whereas $B^n(\vec{\phi}^*)$ can be replaced by the given g^{n+1}.

When B^n and L_2^n do not commute, an approximate solution $\vec{\psi}^*$ can be computed instead of $\vec{\psi}$, where $\vec{\psi}^*$ satisfies

$$B^n(\vec{\psi}^*) = g^{n+1} - g^n \quad , \tag{17a}$$

$$\vec{\psi}^* = \psi + O[\Delta t\|\vec{\phi}^* - \vec{\phi}^n\|] \quad , \tag{17b}$$

instead of Eq. (16). This is, of course, equivalent to using uncorrected (i.e., "physical") boundary conditions for $(\vec{\phi}^* - \vec{\phi}^n)$ as boundary conditions for $\vec{\psi}$. Substituting Eq. (17b) into Eqs. (15) shows that an additional error of order $\Delta t\|\vec{\phi}^* - \vec{\phi}^n\|$ is introduced by the use of "uncorrected" boundary conditions as in Eq. (17a). The overall accuracy in terms of approximating Eq. (11) is $O[\Delta t^2, (\beta-1/2)\,\Delta t, \|\vec{\phi}^* - \vec{\phi}^n\|]$, where, in turn, $\|\vec{\phi}^* - \vec{\phi}^n\|$ is of order Δt. Note, however, that in the steady state $(\vec{\phi}^* - \vec{\phi}^n) \equiv \vec{0}$, and Eq. (17a) becomes an exact boundary condition. Consequently, leaving boundary conditions uncorrected as in Eq. (17a), introduces no error in steady solutions, which, in turn, satisfy $D(\vec{\phi}^*) = \vec{\phi}$. It is worth noting that unless the solution $\vec{\phi}$ of $D(\vec{\phi}^*) = \vec{0}$ is unique, the steady solution $\vec{\phi}^*$ obtained need not be the same as would be obtained by repeating Eq. (11) until $\vec{\phi}^{n+1} - \vec{\phi}^n = \vec{0}$. This completes the derivation of the scheme (15a) and (15b) and its boundary conditions.

Three-point central spatial differences have been employed at all interior grid points in the difference mesh. At the boundaries of the computational domain, second-order accurate three-point, one-sided, spatial differences are used to represent first derivatives where required. An artificial dissipation term based upon a cell Reynolds number criterion has been selectively introduced into the scheme to allow calculations to be performed at high local values of the cell Reynolds numbers.

The coordinate system for interior ballistics calculations must have the ability to enlarge the physical extent of the computational domain as the projectile moves down the gun tube. To accommodate this constraint, an accordion-type mesh is used in the axial direction; i.e., the first and last axial grid points are attached to the breech and projectile, respectively; and the mesh expands as the projectile accelerates down the gun tube. This transformation is $\eta = (z-z_o)/(z_p(t)-z_o)$, where z_o, z, $z_p(t)$ are the axial physical distances to the breech, to the grid point, and to the projectile base, respectively. Transformations are required to refine the computational mesh to regions of large gradients, such as near the walls and where propagating pressure waves appear during the ignition phase of the ballistic cycle. These exponential grid point concentrations are listed in Refs. 7 and 8.

IV. THE MODEL PROBLEM

Because the phenomena occurring in a two-phase, multidimensional interior ballistics environment are extremely complex, an idealized gun system, a one-phase flow in the Lagrange gun, has been simulated to facilitate the understanding of some of the basic mechanisms present in a real gun. The Lagrange gun is a smooth tube of constant radius which is closed at one end by the breech. The combustion chamber, formed by the breech, the initial position of the flat-based projectile, and the tube wall, is filled with a high pressure, high temperature gas which is at rest. The ballistic cycle of this idealized gun resembles that of a real gun if the propellant is assumed to be completely burned before the projectile moves. The projectile is released at time t=0. Frictional forces between the tube wall and the projectile are neglected.

At the present stage of the development, we report on the results of three simulations: the laminar flow-adiabatic wall, the turbulent flow-adiabatic wall, and the laminar flow-isothermal wall. While recognizing that the flow in the Lagrange gun is turbulent and heat loss through the walls does affect the flow field, these simulations isolate the effects of those phenomena and can help in the validation of future codes. A turbulent isothermal computation is in progress. The core flow under laminar-adiabatic assumptions has been verified by an analytic solution and the other cases display the expected trends in the flow field. These benchmark calculations assume cylindrical symmetry and solve the continuity equation, Eq. (1), the Navier-Stokes equations, Eqs. (3), and the energy equation, Eq. (5), with the porosity set to one. The single species gas obeys the Noble-Abel equation of state, Eq. (38), Sutherland's laws for viscosity, Eq. (25), and thermal conductivity, Eq. (36), and Fourier's law of heat conduction, Eq. (34), with α=1. For the turbulent flow calculations, these equations are augmented[13] by the turbulent kinetic energy equation, Eq. (6), and the equations for turbulent viscosity, Eqs. (27), turbulent thermal conductivity,

---

[13] *B.E. Launder and D.B. Spalding, "The Numerical Computation of Turbulent Flows," Computer Methods in Applied Mechanics and Engineering, Vol. 3, pp. 269-289, 1974.*

Eq. (37), and the turbulent heat flux vector, Eq. (35). The mixing length ℓ was set proportional to the distance from the confining surface and a van Driest-type of damping was added to account for viscous effects.

The following boundary conditions are imposed: at the breech, projectile, and tube wall, a no-slip condition is maintained, and the density is determined from the normal momentum equation. The boundary conditions along the centerline of the tube are the symmetry conditions $u=0$, $\partial w/\partial r=0$, $\partial T/\partial r=0$, and $\partial \rho/\partial r=0$. The temperature boundary condition at the solid boundaries is that the normal derivatives of the temperature are set equal to zero for the adiabatic simulations and alternatively the temperature is set equal to 300 K for the isothermal case. In the turbulence simulation, the turbulent kinetic energy and the mixing length are zero on all solid surfaces. To start the turbulence calculations, a small turbulent kinetic energy must be assumed to be present at time t=0. The gun tube geometry, gas properties, and initial conditions are the same for each simulation and are given in Table 1.

TABLE 1. PARAMETERS FOR THE LAGRANGE GUN SIMULATIONS

Bore Diameter	20 mm
Combustion Chamber Length	0.175 m
Maximum Travel of Projectile	1.115 m
Projectile Mass	0.120 kg
Covolume	1.08×10^{-3} m^3/kg
Ratio of Specific Heats	1.271
Initial Gas Pressure	300 MPa
Initial Gas Temperature	3000 K

The axial domain is uniformly divided with 49 mesh lines. The radial domain is nonuniformly divided with 19 mesh lines and with a mesh line concentration near the tube wall, where the first mesh line is at the wall, the second mesh line is 7.7 μm away from the wall, the tenth mesh line is 0.8 mm away from the wall, and the nineteenth mesh line is the centerline of the gun tube.

A. Laminar Flow-Adiabatic Wall Simulation

The dominant features of the one-phase flow within the Lagrange gun are the existence of the rarefaction wave propagation and the development of the velocity and thermal boundary layers along the gun tube wall. The rarefaction

wave is generated by the motion of the projectile and may traverse the distance between the breech and projectile one or more times before the projectile exits the tube. The ALPHA computed pressure histories at the center of the breech and projectile base are given in Figure 2. As predicted in 1793 by Lagrange[14], using many simplifying assumptions and a lumped parameter analysis, the pressure at the breech is always larger than that at the projectile base for this idealized gun system. The position of the rarefaction wave is indicated by a very rapid change in the slope of the pressure curve. In numerical solutions, such changes are often smeared out. The first arrival of the rarefaction wave at the breech and projectile base is captured by the numerics as seen in Figure 2. In the core region, the flow is predominantly axial and at early times is nearly isentropic. A one-dimensional analytic solution for the isentropic case is developed in Ref. 15. The computed pressure values at the time of the rarefaction wave at the breech and projectile are compared to the analytically determined values in Figure 2. The differences between the values are 2.8 percent at the breech and 3.4 percent at the projectile base. The numerical results were obtained with a constant time-step of 10 μs.

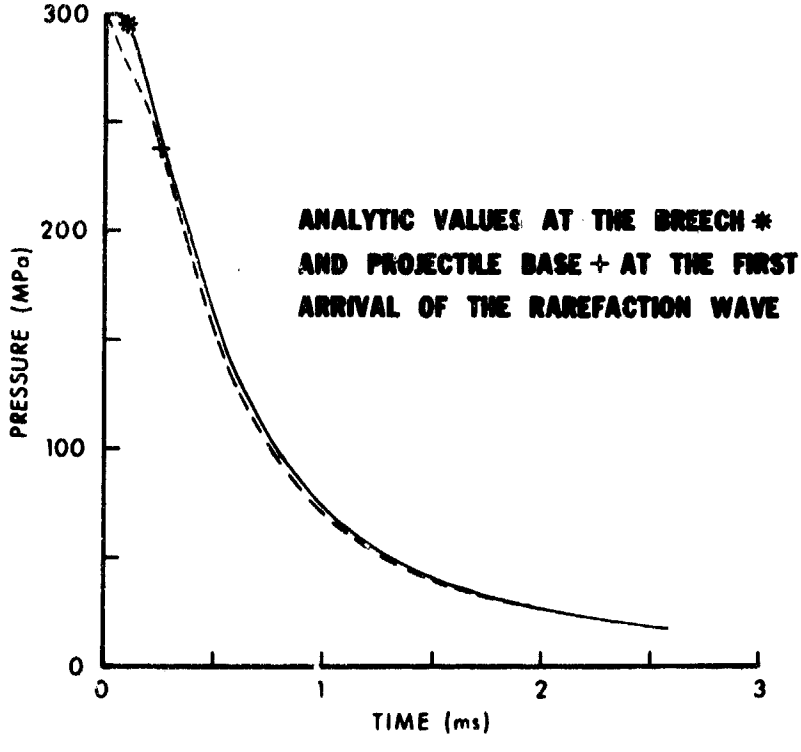

Figure 2. Pressure Histories at the Breech(___) and at Projectile Base(---), and Their Comparisons with Analytically Predicted Initial Arrival Times of the Rarefaction Wave

---

[14] *J. Corner, Theory of Interior Ballistics of Guns, Wiley, New York, pp. 339-356, 1950.*

[15] *E.H. Love and F. B. Pidduck, "Lagrange's Ballistic Problem," Phil. Trans. Roy. Soc., Vol. 222, pp. 167-226, 1921-22.*

The gun geometry, gas parameters, initial conditions, and boundary conditions used in the simulation are identical to those used by Heiser and Hensel[16]. Despite these similarities, the results of the simulations differed greatly[17]. Subsequent results from West Germany[18] show agreement between the simulations. For example, at a muzzle-time of 2.6 ms, the differences between these calculations at the projectile base are 0.4 percent in the temperature, 0.8 percent in the axial displacement values, and 2.2 percent in the velocity values.

The other dominant features of the flow field within the Lagrange gun are the boundary layers along the gun tube wall. The velocity boundary layer profiles at time 2.4 ms are given in Figure 3, where z_p and w_p denote the axial position and velocity of the projectile, respectively. The 99 percent velocity boundary layer thickness has a maximum value along the tube of 0.19 mm. A more physically meaningful measurement for the boundary layer thickness is the displacement thickness δ. For compressible flows with cylindrical geometry, it is defined at time t and position z as

$$\delta(z,t) = \int_0^R \left[1 - \frac{w(r,z,t)}{w_c(z,t)} \frac{\rho(r,z,t)}{\rho_c(z,t)}\right] \frac{r}{R}\, dr \ , \qquad (18)$$

where the subscript c denotes the value at the centerline, w is the axial velocity, ρ is the density, and R is the tube radius. The displacement thickness values given in Table 2 are approximately 27 percent of the 99 percent velocity boundary layer thickness values. At 2.4 ms, the maximum displacement thickness occupies less than 0.6 percent of the gun diameter. The thermal boundary layers at 2.4 ms are given in Figure 4. The core temperatures decrease as a function of the distance from the breech due to the motion of the projectile. The temperature profile at the projectile base is approximately constant in the radial direction. Along the adiabatic tube wall, the viscous heating raises the wall temperature to a maximum value away from the projectile base, e.g., in Figure 4 at Z = 0.805 m. The wall temperature then decreases from this concentrated region of high temperature as one proceeds to the breech.

---

[16] *R. Heiser and D. Hensel, "Calculation of the Axisymmetric Unsteady Compressible Boundary Layer Flow Behind a Moving Projectile," Proceedings of the Fourth International Symposium on Ballistics, 1978, American Defense Preparedness Association, Washington, DC.*

[17] *J.A. Schmitt and T.L. Mann, "Calculation of the Compressible Flow in the Lagrange Gun by the Interior Ballistics Algorithm, ALPHA," Proceedings of the DEA-G-1060 Meeting at Eglin Air Force Base, October 1980, Air Force Armament Division, Eglin Air Force Base, Florida, pp. 4-28.*

[18] *R. Heiser and D. Hensel, "Berechnung der Gasstromung in einem Waffenrohr mit Hilfe des Zweidimensionalen AMI-Modells," E1/81, January 1981, Ernst-Mach-Institut, Abteilung fuer Ballistik, Weil am Rhein, West Germany.*

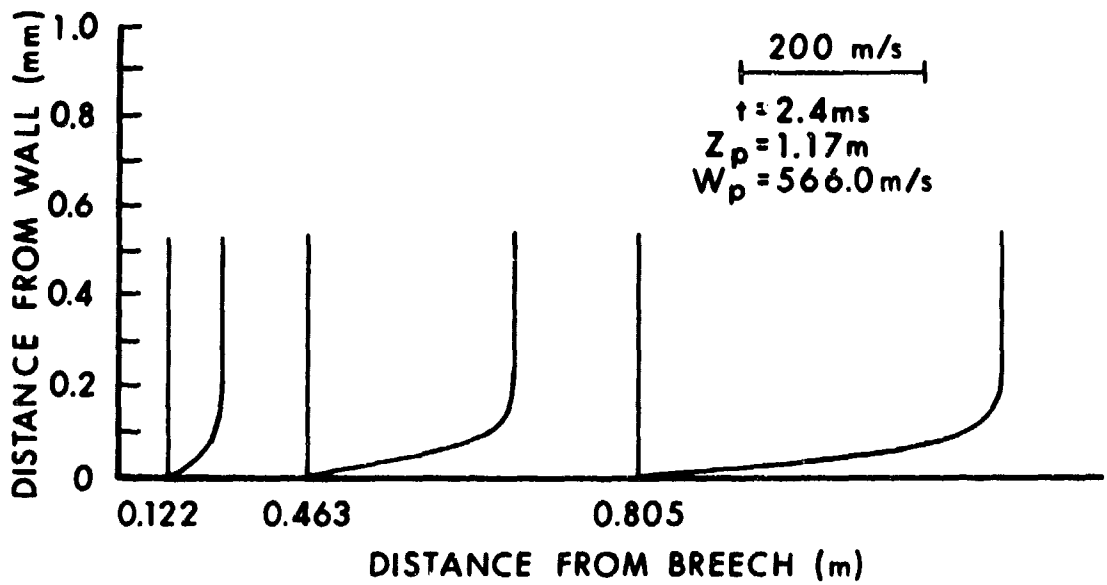

Figure 3. Velocity Boundary Layer Profiles for the Laminar Flow-Adiabatic Wall Calculation

TABLE 2. DISPLACEMENT THICKNESSES IN THE LAGRANGE GUN AT TIME t=2.4 ms

Distance from Breech (m)	Displacement Thickness (mm) Laminar-Adiabatic Case	Turbulent-Adiabatic Case	Laminar-Isothermal Case
.073	.052	.094	.005
.268	.052	.161	.002
.439	.052	.193	.002
.634	.050	.210	.002
.805	.046	.216	0

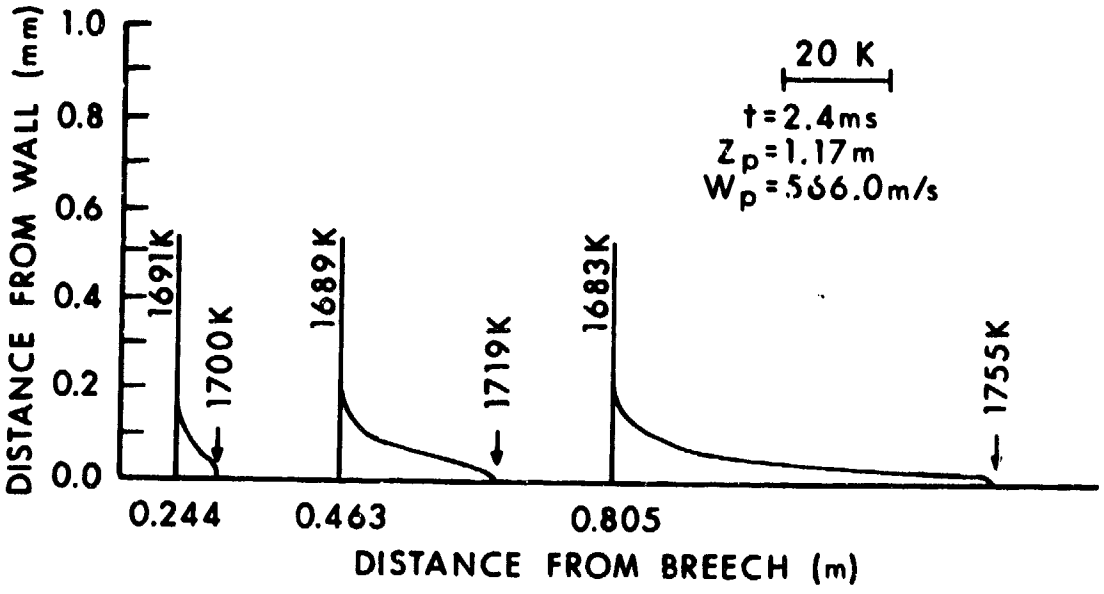

Figure 4. Thermal Boundary Layer Profiles for the Laminar Flow-Adiabatic Wall Calculation

B. Turbulent Flow-Adiabatic Wall Simulation

Indications are that the flow in a gun barrel, even in an idealized Lagrange gun, is turbulent. Thus, a k-ℓ turbulence model was incorporated into the computational scheme and the results compared with the laminar runs to determine if there are significant differences.

Perhaps the most interesting result of the turbulence simulation is the displacement layer (Table 2). At muzzle time, at a distance of 0.8 m from the breech, the displacement thickness is 0.2 mm. The velocity profiles, Figure 5, are typical of turbulent flow. As a conse[illegible]nce of the viscous heating along the adiabatic wall, there is a negativ[illegible]emperature gradient in the direction away from the wall; for example, at 0.8 m from the breech, the wall temperature is 1742 K while the centerline is still at 1690 K (Figure 6). Note that the scale of the ordinate in the figure is so large that the actual grid spacing of the computational domain can no longer be discerned near the wall. An enlarged view would show that the adiabatic wall condition $\frac{\partial T}{\partial r} = 0$ is strictly maintained. The level of turbulence, measured by the turbulent kinetic energy, increases from the breech toward the projectile. The mixing action of the turbulence transports heat from the viscous region near the wall into the core flow which is reflected in the temperature gradient seen in Figure 6.

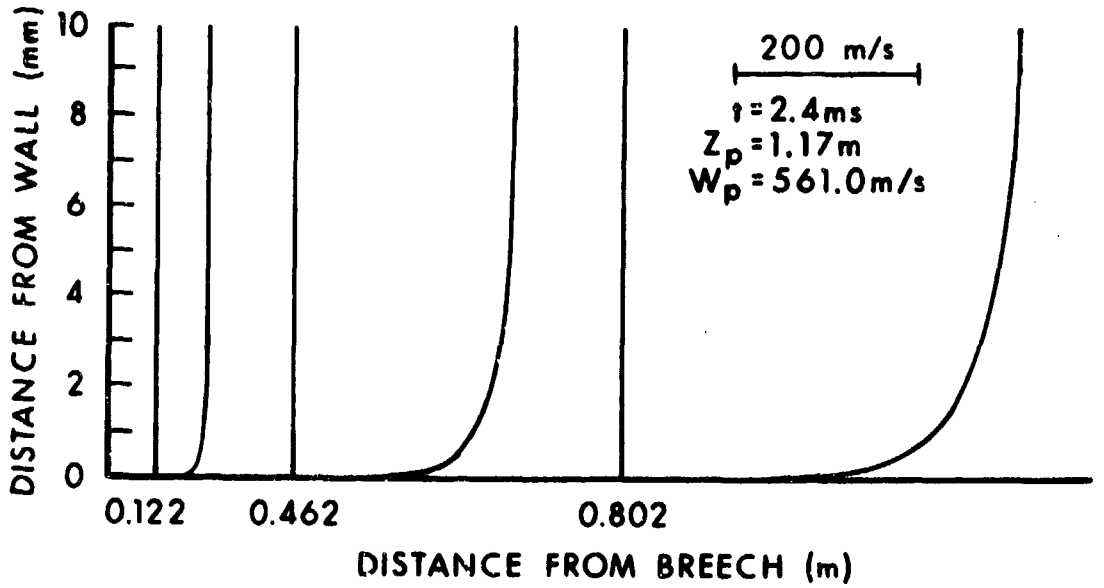

Figure 5. Velocity Boundary Layer Profiles for the Turbulent Flow-Adiabatic Wall Calculation

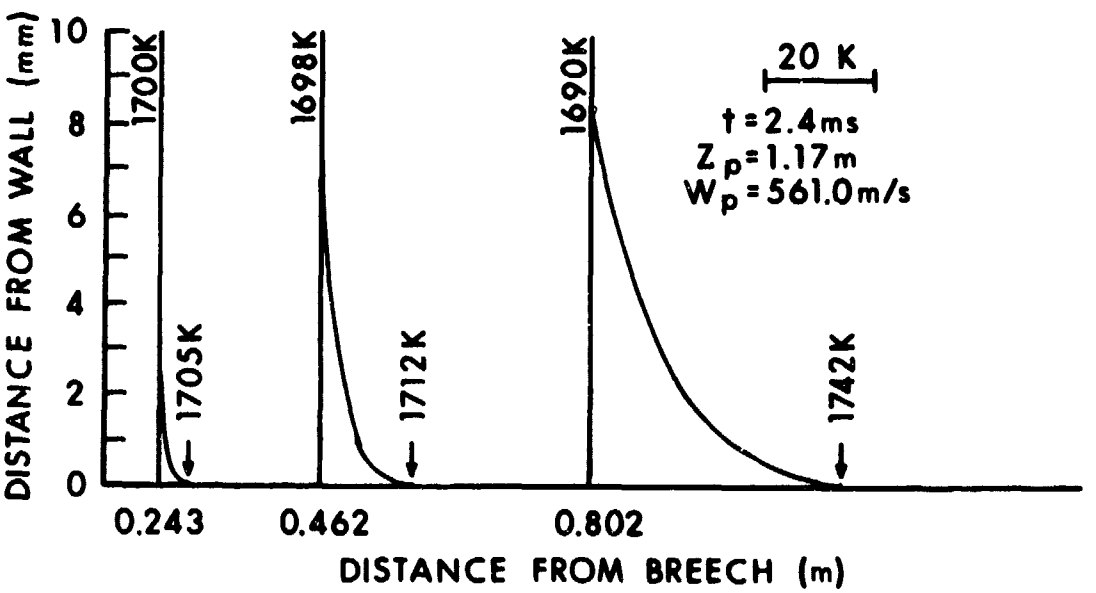

Figure 6. Thermal Boundary Layer Profiles for the Turbulent Flow-Adiabatic Wall Calculation

C. Laminar Flow-Isothermal (Cold Wall) Simulation

The simulation of the laminar flow in the Lagrange gun, under isothermal wall conditions, determines the effects of heat losses on the dynamics of the flow field and the motion of the projectile. This simulation is a reasonable approximation of the heat transfer for the real case of a turbulent flow with heat conducting walls. The calculations predict that approximately 20 percent of the total energy available in the gas is lost through the cold walls. These results are in agreement with predicted heat losses from conventional propellants in medium caliber guns[1].

Radial dependence of the axial velocity profiles as a function of distance from the breech of the gun is shown in Figure 7. The maximum value of the 99 percent velocity boundary layer thickness is calculated to be 0.15 mm. The corresponding displacement thicknesses are given in Table 2. The 99 percent velocity boundary layer thicknesses of this case are comparable to those of the laminar flow-adiabatic wall simulation. However, the corresponding displacement thicknesses differ by over an order of magnitude because the density variation is taken into account in the displacement thickness calculation whereas it is not in the 99 percent velocity boundary layer computation. See Eq. (18). The gas density near the wall for the isothermal cold wall case is significantly different from the adiabatic case because the pressure values are approximately the same but the temperature values differ greatly. In general, the thermal boundary layer in the cold wall simulation remain extremely steep over the time span of in-bore travel (Figure 8).

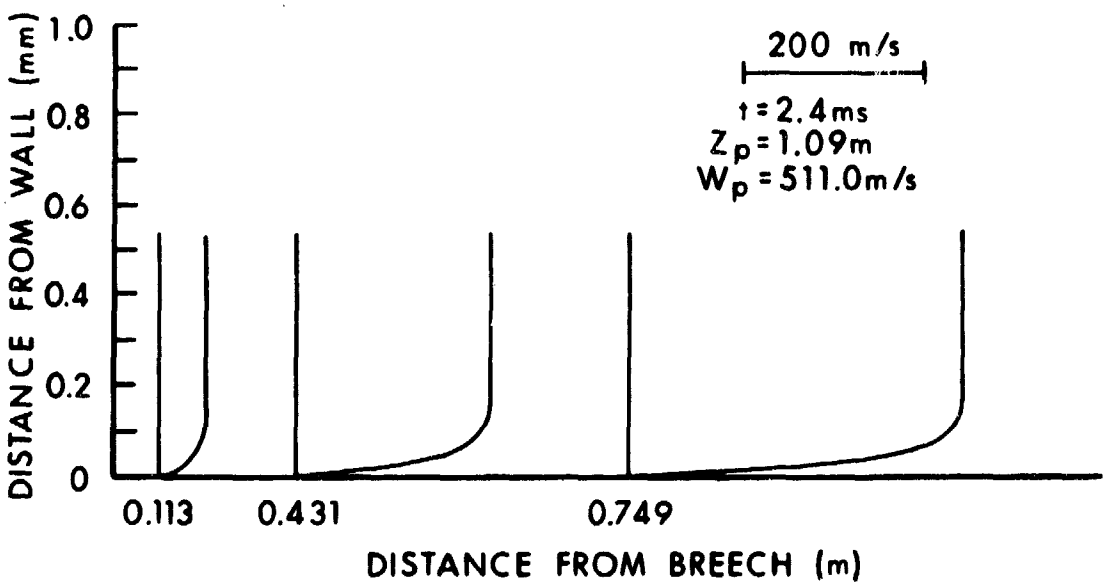

Figure 7. Velocity Boundary Layer Profiles for the Laminar Flow-Isothermal (Cold Wall) Calculations

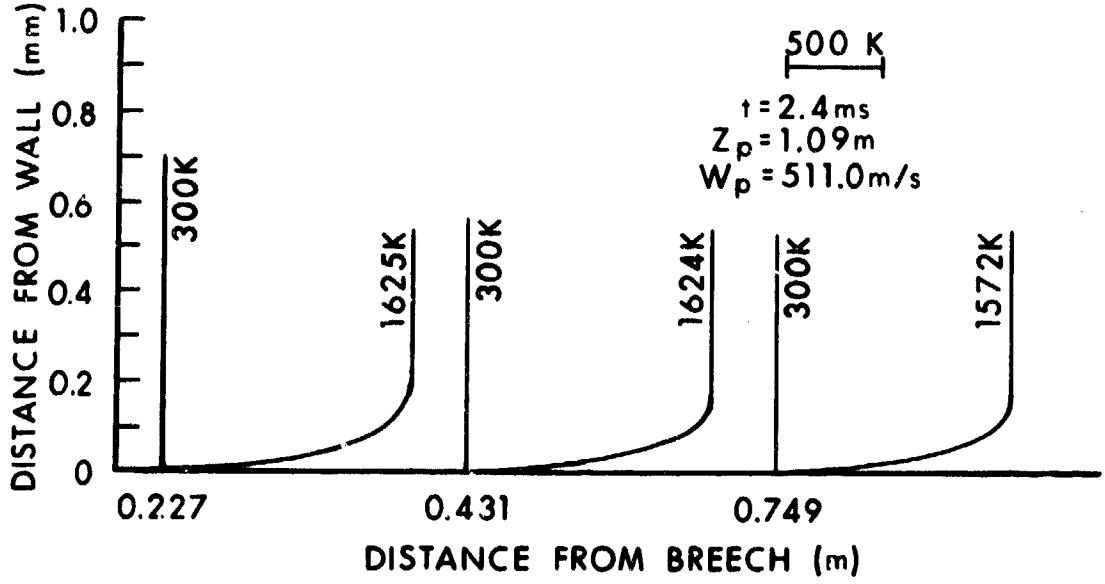

Figure 8. Thermal Boundary Layer Profiles for the Laminar Flow-Isothermal (Cold Wall) Calculation

During the early transients, the discontinuity in the initial conditions for the temperature creates a strong transient "thermal discontinuity" in the chamber cavity. This results from the drop in temperature through the thin layer of gas adjacent to the wall, which is needed to satisfy the boundary condition while keeping the pressure at 300 MPa. Consequently, severe gradients in the gas density near the walls occur and the convection and diffusion of the mass to these regions persist for most of the in-bore travel time.

D. Comparison Among the Simulations

From the results we see that there are some significant differences in the flow fields of the three cases. Calculations with a turbulence model reveal marked departures from the laminar case in the details of the flow, although the overall trends are similar. The isothermal case differs on both the micro and the macro scale. For the adiabatic wall, the velocity profile normal to the tube wall is more gradual for a turbulent calculation than the corresponding laminar one with a corresponding thickening of the displacement thickness. In fact, for example, at a distance of 0.4 m from the breech (Figure 9) the turbulent displacement thickness is 0.19 mm while the corresponding laminar value is 0.05 mm. Due to the eddy motion in the turbulence, there is a considerable mixing of fluid leading to a lower temperature at the wall and a more rapid transport of heat into the core (Figure 4 and 6). In the cold wall case, the displacement thickness is very thin, of the order of 0.005 mm at 10 mm from the breech near projectile exit time, and gets progressively thinner as one moves toward the projectile (Figure 9).

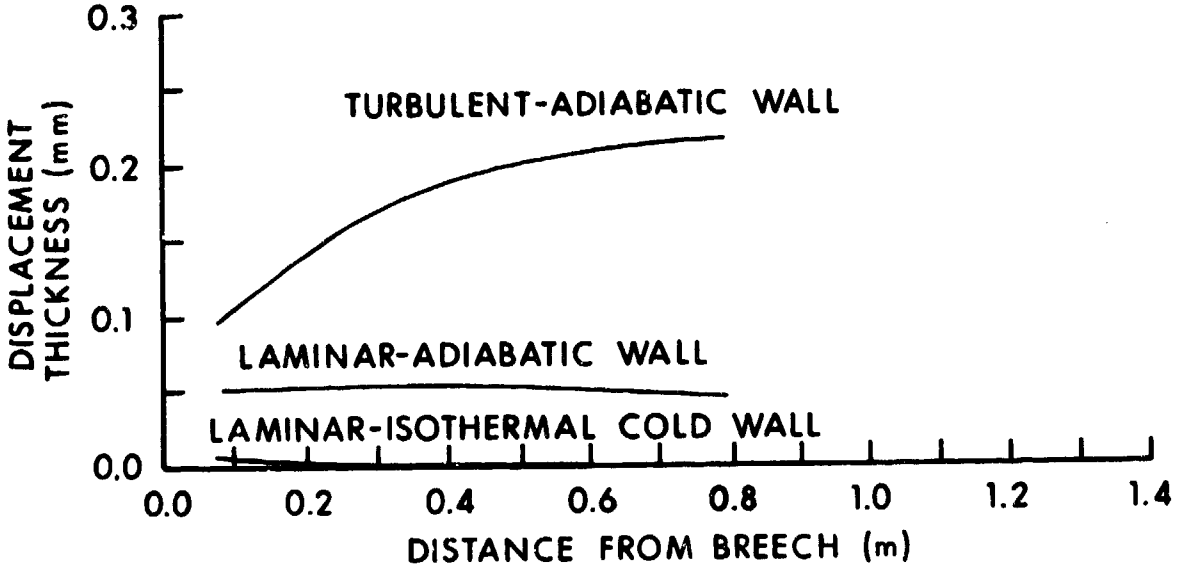

Figure 9. Comparisons of the Displacement Thicknesses for the Three Simulations of the Model Lagrange Gun Problem at t=2.4 ms

From Figure 10, we see that the projectile velocity in the turbulent case is slightly lower than in the laminar case and the velocity difference increases as the projectile travels down the tube, confirming the fact that energy is taken up by the turbulent motion and, thus, demonstrating the consistency of the results. The difference between the adiabatic and the isothermal cold wall projectile velocities for the laminar simulation is quite large and increases with time. Due to the loss of energy through the solid surfaces during in-bore travel time, the muzzle velocity in the cold wall case is 50 m/s less than in the adiabatic case. Furthermore, this heat loss causes a notable temperature difference along the centerline between these cases which can be seen by comparing Figures 4 and 8. At about 70 percent of the distance from the breech to the projectile base, the temperature difference is approximately 110 K. In the adiabatic cases (Figures 4 and 6), heat generated by the viscous heating at the wall is transported and conducted into the flow leading to the positive temperature gradient as one approaches the wall. Whereas in the isothermal case (Figure 8), heat is lost through the wall leading to a negative temperature gradient.

V. CONCLUSIONS AND FUTURE EFFORTS

An advancement has been made in the state-of-the-art in modeling computationally the multidimensional interior ballistics of high-velocity guns. The numerical LBI scheme is used to solve the axisymmetric, two-phase, averaged Navier-Stokes equations which describe the transient flow behind an accelerating projectile. However, in the first application of this algorithm, the interior ballistics flow has been idealized to a single-phase case; and three simulations are presented: a laminar flow with an adiabatic wall

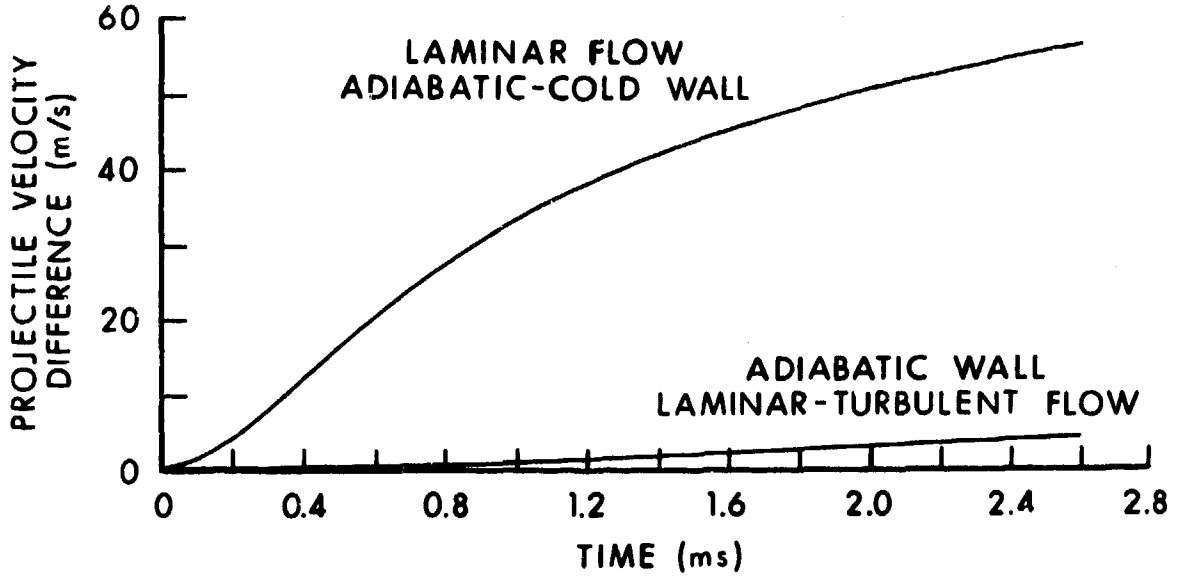

Figure 10. Differences in Projectile Velocities as a Function of Time, Flow, and Boundary Conditions

condition, a turbulent flow with an adiabatic wall condition, and a laminar flow with an isothermal cold wall condition. Despite a relatively coarse mesh, the rarefaction wave has been captured; the projectile motion has been successfully coupled to the two-dimensional flow field; and the velocity and thermal profiles, as well as displacement thicknesses, have been determined for all the cases. Comparisons with analytical results and others, when available, have resulted in excellent agreement. Furthermore, confidence in these results were enhanced through time-step and mesh refinements.

Past attempts to model the viscous flow within an idealized ballistic cycle has been confined to boundary layer studies via the boundary layer equations[19]. They predict trends analogous to those reported here; such as, the thickening of the boundary layer along the tube wall under turbulent conditions. However, because those approaches fail to consider the entire flow and the flow-projectile interaction, they cannot simulate the decrease in the projectile velocity due to turbulence or heat transfer to the wall. These effects can be significant.

In the one-phase simulations reported here, important aspects of the two-phase flow were excluded from the initial validation of the basic models and the algorithm. The next step in the development of the viscous simulation of the ballistic cycle is the inclusion of the solid phase in the Lagrange gun and the validation of the corresponding two-phase models. To this end, benchmark experiments in a well-controlled ballistic environment are being designed in conjunction with the modeling efforts. Two of the most pressing needs in the modeling effort in two-phase flow are the development of models of turbulence for the second phase and a more realistic description of the interaction between phases.

---

[19] *E.P. Bartlett, L.W. Anderson, and R.M. Kendall, "Time-Dependent Boundary Layers with Application to Gun Barrel Heat Transfer,"* Proceedings of Twelfth Heat Transfer and Fluid Mechanics Institute, *Stanford University Press, pp. 262-278, 1972.*

REFERENCES

1. H. Krier and M. Adams, "An Introduction to Gun Interior Ballistics and a Simplified Ballistic Code," Interior Ballistics of Guns, H. Krier and M. Summerfield, Eds., Progress in Astronautics and Aeronautics, Vol. 66, pp. 1-36, 1979.

2. P.S. Gough and F.J. Zwarts, "Modeling Heterogeneous Two-Phase Reacting Flow," AIAA Journal, Vol. 17, No. 1, pp. 17-25, 1979.

3. K.K. Kuo, J.H. Koo, T.R. Davis, and G.R. Coates, "Transient Combustion in Mobile Gas-Permeable Propellants," Acta Astronautica, Vol. 3, pp. 573-591, 1976.

4. E.B. Fisher, K.W. Graves, and A.P. Trippe, "Application of a Flame Spread Model to Design Problems in the 155-mm Propelling Charge," 12th JANNAF Combustion Meeting, CPIA Pub. 273, Vol. I, pp. 199-219, December 1975.

5. H. Krier and S.S. Gokhale, "Modeling of Convective Mode Combustion Through Granulated Propellant to Predict Detonation Transition," AIAA Journal, Vol. 16, No. 2, pp. 177-183, 1978.

6. P.S. Gough, "A Two-Dimensional Model of the Interior Ballistics of Bagged Artillery Charges," USA ARRADCOM/Ballistic Research Laboratory, Aberdeen Proving Ground, MD, ARBRL-CR-00452, April 1981.

7. H.J. Gibeling, R.C. Buggeln, and H. McDonald, "Development of a Two-Dimensional Implicit Interior Ballistics Code," US Army ARRADCOM/Ballistic Research Laboratory, Aberdeen Proving Ground, MD, ARBRL-CR-00411, January 1980.

8. H.J. Gibeling and H. McDonald, "Development of a Two-Dimensional Implicit Interior Ballistics Code," US Army ARRADCOM/Ballistic Research Laboratory, Aberdeen Proving Ground, MD, ARBRL-CR-00451, March 1981.

9. D. Drew, Rennsselaer Polytechnic Institute, Private Communication, June 1981.

10. W.R. Briley and H. McDonald, "Solution of the Multidimensional Compressible Navier-Stokes Equations by a Generalized Implicit Method," Journal of Computational Physics, Vol. 24, No. 4, pp. 372-397, 1977.

11. W.R. Briley and H. McDonald, "On the Structure and Use of Linearized Block ADI and Related Schemes," Journal of Computational Physics, Vol. 34, No. 1, pp. 54-73, 1980.

12. H. McDonald and W.R. Briley, "Some Observations on Numerical Solutions of the Three-Dimensional Navier-Stokes Equations," presented at Symposium on Numerical and Physical Aspects of Aerodynamic Flows, California State University, Long Beach, CA 1981.

13. B.E. Launder and D.B. Spalding, "The Numerical Computation of Turbulent Flows," Computer Methods in Applied Mechanics and Engineering, Vol. 3, pp. 269-289, 1974.

14. J. Corner, Theory of Interior Ballistics of Guns, Wiley, New York, pp. 339-356, 1950.

15. E.H. Love and F.B. Pidduck, "Lagrange's Ballistic Problem," Phil. Trans. Roy. Soc., Vol. 222, pp. 167-226, 1921-22.

16. R. Heiser and D. Hensel, "Calculation of the Axisymmetric Unsteady Compressible Boundary Layer Flow Behind a Moving Projectile," Proceedings of the Fourth International Symposium on Ballistics, American Defense Preparedness Association, Washington, DC, 1978.

17. J.A. Schmitt and T.L. Mann, "Calculation of the Compressible Flow in the Lagrange Gun by the Interior Ballistics Algorithm, ALPHA," Proceedings of the DEA-G-1060 Meeting at Eglin Air Force Base, pp. 4-28, October 1980.

18. R. Heiser and D. Hensel, "Berechnung der Gasströmung in einem Waffenrohr mit Hilfe des Zweidimensionalen AMI-Modells," Ernst-Mach-Institut, Abteilung fuer Ballistik, Weil am Rhein, West Germany, E1/81, January 1981.

19. E.P. Bartlett, L.W. Anderson, and R.M. Kendall, "Time-Dependent Boundary Layers with Application to Gun Barrel Heat Transfer," Proceedings of Twelfth Heat Transfer and Fluid Mechanics Institute, Stanford University Press, pp. 262-278, 1972.

APPENDIX

CORRELATIONS AND CONSTITUTIVE LAWS

In this Appendix, we list the constitutive laws and the correlations needed to close the two-phase model. The mass source due to the propellant burning is

$$\Gamma = (1-\alpha) \frac{S_p \rho_p}{V_p} \langle d \rangle \quad , \tag{19}$$

where the grain surface area, grain volume, and regression rate are

$$S_p = 4\pi r_p^2 \quad , \tag{20}$$

$$V_p = \frac{4}{3} \pi^3_p \quad , \tag{21}$$

$$\langle d \rangle = B_1 + B_2 P^n \quad , \tag{22}$$

respectively. The constants B_1, B_2, and n are known for a given propellant. The gas phase stress tensor, assuming a Newtonian fluid, is

$$\bar{\bar{\pi}} = 2\mu \bar{\bar{D}} - (\frac{2}{3}\mu - K_B) \nabla \cdot \vec{U} \bar{\bar{\Pi}} \quad , \tag{23}$$

where μ is the molecular viscosity, K_B is the bulk viscosity and $\bar{\bar{\Pi}}$ is the identity tensor. The rate of strain tensor $\bar{\bar{D}}$ is given as

$$\bar{\bar{D}} = 0.5 \left[\nabla \vec{U} + (\nabla \vec{U})^{\text{transpose}}\right] \quad . \tag{24}$$

The molecular viscosity μ is determined from Sutherland's law

$$\frac{\mu}{\mu_o} = (\frac{T}{T_o})^{3/2} \frac{T_o + S_1}{T + S_1} \quad , \tag{25}$$

where $S_1 = 110$ K and the subscript zero indicates some reference quantity. The bulk viscosity K_B is assumed to be zero. The turbulent stress tensor is modeled using an isotropic eddy viscosity formulation

$$\bar{\bar{\pi}}^T = 2\mu^T \bar{\bar{D}} - \frac{2}{3} (\mu^T \nabla \cdot \vec{U} + \rho k) \bar{\bar{\Pi}} \quad , \tag{26}$$

$$\mu^T = \rho c_\mu \frac{k^2}{\varepsilon} \quad , \tag{27}$$

$$\varepsilon = c_\mu^{3/4} \frac{k^{3/2}}{\ell} \quad , \tag{28}$$

where ℓ is the mixing length and c_μ is a function of the turbulent Reynolds number. The interphase drag relation $\langle \vec{F} \rangle$ is given by

$$\langle \vec{F} \rangle = \frac{\rho(\vec{U}-\vec{U}_p) \; \|\vec{U}-\vec{U}_p\|}{6} \hat{f} \quad , \text{ where}$$

$$\hat{f} = \begin{cases} 1.75 & \alpha < \alpha_c \\ 1.75 \left[\frac{1-\alpha}{1-\alpha_c} \frac{\alpha_c}{\alpha}\right]^{0.45} & \alpha_c < \alpha < \alpha_1 \\ 0.3 & \alpha_1 < \alpha < 1 \end{cases} \quad , \tag{29}$$

$$\alpha_1 = \left[1 + 0.01986 \left(\frac{1-\alpha_c}{\alpha_c}\right)\right]^{-1} \quad ,$$

where α_c is the settling porosity of the propellant bed. The intergranular stress relation R_p which is independent of the loading density history is given by

$$R_p = \begin{cases} -\rho_p a_p^2 \frac{\alpha_c - \alpha}{1-\alpha} \frac{\alpha_c}{\alpha} , & \alpha \leq \alpha_c \\ 0 , & \text{else} \end{cases} \quad , \tag{30}$$

where a_p is the speed of sound in the solid phase which is specified for a given propellant. The dissipation function Φ is given by

$$\Phi = 2\mu \, \overline{\overline{D}} : \overline{\overline{D}} - \left(\frac{2}{3}\mu - K_B\right) (\nabla \cdot \vec{U})^2 \quad . \tag{31}$$

The interfacial energy transfer Λ is given by

$$\Lambda = -P (\vec{U}-\vec{U}_p) \cdot \nabla \alpha + (1-\alpha) \frac{S_p}{V_p} (\vec{U}-\vec{U}_p) \cdot \langle \vec{F} \rangle + \vec{q} \cdot \nabla \alpha - (1-\alpha) \frac{S_p}{V_p} \langle \vec{q} \rangle \tag{32}$$

$$+ \Gamma \left[h_{comp} + \frac{1}{2} (\vec{U}-\vec{U}_p) \cdot (\vec{U}-\vec{U}_p)\right] \quad ,$$

where h_{comp} is the energy released per unit mass due to combustion of the propellant. The interfacial heat transfer $\langle q \rangle$ is given by

$$\langle q \rangle = h_t (T - T_{ps}) \quad ,$$

$$\text{where } h_t = \frac{K}{2r_p} Nu_p + \varepsilon_p \sigma (T+T_{ps})(T^2+T_{ps}^2) \quad ,$$

$$Nu_p = 2.0 + 0.4 \, Re_p^{2/3} \, Pr^{1/3} \quad , \tag{33}$$

$$Re_p = \frac{2r_p \rho \| \vec{U} - \vec{U}_p \|}{\mu} \quad ,$$

where ε_p = propellant emissivity, σ = Stefan-Boltzmann constant, and $Pr = \mu c_p / K$. The surface temperature of the propellant T_{ps} is computed from the solution of Eq. (9). The laminar and turbulent heat flux vector can be modeled as

$$\vec{q} = - K \left[\nabla T - \frac{\nabla \alpha}{\alpha} (T_i - T) \right] \quad , \tag{34}$$

and

$$\vec{q}^T = - K^T \left[\nabla T - \frac{\nabla \alpha}{\alpha} (T_i - T) \right] \quad , \tag{35}$$

respectively, where $T_i = 0.5(T+T_{ps})$. The thermal conductivity K is determined from Sutherland's law

$$\frac{K}{K_o} = \left(\frac{T}{T_o} \right)^{3/2} \frac{T_o + S_2}{T + S_2} \quad , \tag{36}$$

where $S_2 = 194$ K and subscript zero indicates some reference quantity. The turbulent thermal conductivity is given by

$$K^T = c_p \mu_{eff} / Pr_{eff} - K \quad , \tag{37}$$

where $Pr_{eff} = 0.9$. The Noble-Abel equation of state is

$$P(1 - \rho\eta) = \rho M T R_u \quad , \tag{38}$$

where η is the covolume factor which provides a correction to the perfect gas equation of state needed for gases with large density and R_u is the universal gas constant. Other thermodynamic properties are

$$c_p = c_v + MR_u \quad , \quad \gamma = c_p/c_v \quad , \tag{39}$$

and

$$h = c_p T + \eta P \quad . \tag{40}$$

NOMENCLATURE

a_p = speed of sound in the propellant, m/s

B = linearized operator

c_p = specific heat at constant pressure, J/(kg•K)

c_v = specific heat at constant volume, J/(kg•K)

d_p = propellant thermal diffusivity, m^2/s

$\langle d \rangle$ = regression rate of solid phase, m/s

$D(\phi)$ = spatial differential operator

$\bar{\bar{D}}$ = rate of strain tensor, 1/s

$\langle \vec{F} \rangle$ = interphase drag per unit area of solid phase, Pa

h = specific enthalpy, J/kg

I = identity matrix

k = specific turbulent kinetic energy, J/kg

K_B = bulk viscosity, Pa•s

K = laminar thermal conductivity, W/(m•K)

ℓ = turbulent mixing length, m

L = linearized differential operator

M = reciprocal molecular weight of gas mixture, mol/kg

P = pressure, Pa

$\vec{q}$ = laminar heat flux vector, $J/(m^2 \cdot s)$

$\vec{q}^T$ = turbulent heat flux vector, $J/(m^2 \cdot s)$

$\langle q \rangle$ = interfacial heat transfer, $W/(m^2)$

R_p = isotropic intergranular stress, Pa

R_u = universal gas constant, J/(mol•K)

r = radial distance from the centerline in the gun tube, m

r_p = propellant radius, m

S_p = propellant surface area, m^2

Sc_{eff} = 0.9

t = time, s

T = gas temperature, K

T_p = propellant temperature, K

u = radial component of gas velocity, m/s

$\vec{U}$ = gas velocity vector, m/s

$\vec{U}_p$ = propellant velocity vector, m/s

V_p = propellant volume, m^3

w = axial component of gas velocity, m/s

z = axial distance from the breech in the gun tube, m

z_p = axial distance to the projectile base from the breech, m

α = porosity (ratio of gas volume to total averaged volume)

α_c = settling porosity

β = finite difference weighting factor

Γ = mass source due to propellant burning, $kg/m^3 \cdot s$

Γ_m = μ_{eff}/Sc_{eff}

δ = displacement thickness, m

ε = turbulent kinetic energy dissipation rate, $J/(s \cdot kg)$

η = covolume, m^3/kg

Λ = energy transfer between solid and gas phases, $J/(m^3 \cdot s)$

μ = molecular viscosity, $Pa \cdot s$

μ_T = turbulent viscosity, $Pa \cdot s$

μ_{eff} = $\mu + \mu^T$, $Pa \cdot s$

$\overline{\overline{\pi}}$ = laminar stress tensor, Pa

$\overline{\overline{\pi}}^T$ = turbulent stress tensor, Pa

$\overline{\overline{\Pi}}$ = identity tensor

ρ = gas density, kg/m^3

ρ_p = propellant density, kg/m^3

$\vec{\phi}$ = vector of dependent variables

Φ = gas dissipation function, $J/(m^3 \cdot s)$

$\vec{\psi}$ = intermediate variable due to algorithm splitting

DISTRIBUTION LIST

No. of Copies	Organization
12	Administrator Defense Technical Info Center ATTN: DTIC-DDA Cameron Station Alexandria, VA 22314
1	Commander US Army Materiel Development and Readiness Command ATTN: DRCDMD-ST 5001 Eisenhower Avenue Alexandria, VA 22333
1	Commander US Army Armament Research and Development Command ATTN: DRDAR-TDC Dover, NJ 07801
2	Commander US Army Armament Research and Development Command ATTN: DRDAR-TSS Dover, NJ 07801
1	Commander US Army Armament Material Readiness Command ATTN: DRSAR-LEP-L, Tech Lib Rock Island, IL 61299
1	Director US Army ARRADCOM Benet Weapons Laboratory ATTN: DRDAR-LCB-TL Watervliet, NY 12189
1	Commander US Army Aviation Research and Development Command ATTN: DRDAV-E 4300 Goodfellow Blvd. St. Louis, MO 63120
1	Director US Army Air Mobility Research and Development Laboratory Ames Research Center Moffett Field, CA 94035
1	Commander US Army Communications Research and Development Command ATTN: DRDCO-PPA-SA Fort Monmouth, NJ 07703
1	Commander US Army Electronics Research and Development Command Technical Support Activity ATTN: DELSD-L Fort Monmouth, NJ 07703
1	Commander US Army Missile Command ATTN: DRSMI-R Redstone Arsenal, AL 35898
1	Commander US Army Missile Command ATTN: DRSMI-YDL Redstone Arsenal, AL 35898
1	Commander US Army Tank Automotive Research and Development Command ATTN: DRDTA-UL Warren, MI 48090
1	Director US Army TRADOC Systems Analysis Activity ATTN: ATAA-SL, Tech Lib White Sands Missile Range, NM 88022
1	JAYCOR ATTN: James Stuhmiller P.O. Box 85154 San Diego, CA 92138
1	Scientific Research Associates, Inc. ATTN: Henry McDonald P.O. Box 498 Glastonbury, CT 06033

DISTRIBUTION LIST

No. of Copies	Organization	No. of Copies	Organization

Aberdeen Proving Ground

Dir, USAMSAA
ATTN: DRXSY-D
DRXSY-MP, H. Cohen
Cdr, USATECOM
ATTN: DRSTE-TO-F
Dir, USACSL, Bldg. E3516, EA
ATTN: DRDAR-CLB-PA

USER EVALUATION OF REPORT

Please take a few minutes to answer the questions below; tear out this sheet, fold as indicated, staple or tape closed, and place in the mail. Your comments will provide us with information for improving future reports.

1. BRL Report Number _____

2. Does this report satisfy a need? (Comment on purpose, related project, or other area of interest for which report will be used.)

_____

_____

_____

3. How, specifically, is the report being used? (Information source, design data or procedure, management procedure, source of ideas, etc.) _____

_____

_____

4. Has the information in this report led to any quantitative savings as far as man-hours/contract dollars saved, operating costs avoided, efficiencies achieved, etc.? If so, please elaborate.

_____

_____

5. General Comments (Indicate what you think should be changed to make this report and future reports of this type more responsive to your needs, more usable, improve readability, etc.) _____

_____

_____

_____

6. If you would like to be contacted by the personnel who prepared this report to raise specific questions or discuss the topic, please fill in the following information.

Name: _____

Telephone Number: _____

Organization Address: _____

_____

_____

FOLD HERE

Director
US Army Ballistic Research Laboratory
ATTN: DRDAR-BLA-S
Aberdeen Proving Ground, MD 21005

NO POSTAGE
NECESSARY
IF MAILED
IN THE
UNITED STATES

OFFICIAL BUSINESS
PENALTY FOR PRIVATE USE, $300

BUSINESS REPLY MAIL
FIRST CLASS PERMIT NO 12062 WASHINGTON, DC
POSTAGE WILL BE PAID BY DEPARTMENT OF THE ARMY

Director
US Army Ballistic Research Laboratory
ATTN: DRDAR-BLA-S
Aberdeen Proving Ground, MD 21005

FOLD HERE